HHS Public Access

Author manuscript

IEEE Trans Med Imaging. Author manuscript; available in PMC 2018 February 01.

Published in final edited form as:

IEEE Trans Med Imaging. 2017 February ; 36(2): 487–496. doi:10.1109/TMI.2016.2615567.

Using Anatomic Magnetic Resonance Image Information to Enhance Visualization and Interpretation of Functional Images: A Comparison of Methods Applied to Clinical Arterial Spin Labeling Images

Li Zhao,
Department of Radiology, Beth Israel Deaconess Medical Center and Harvard Medical School, Boston, MA, 02215 USA

Weiying Dai,
Department of Radiology, Beth Israel Deaconess Medical Center and Harvard Medical School, Boston, MA, 02215 USA. She is now with the Department of Computer Science, State University of New York at Binghamton, Binghamton, NY, 13902 USA

Salil Soman,
Department of Radiology, Beth Israel Deaconess Medical Center and Harvard Medical School, Boston, MA, 02215 USA

David B. Hackney,
Department of Radiology, Beth Israel Deaconess Medical Center and Harvard Medical School, Boston, MA, 02215 USA

Eric T. Wong,
Department of Neurology, Beth Israel Deaconess Medical Center and Harvard Medical School, Boston, MA, 02215 USA

Philip M. Robson, and
Department of Radiology, Beth Israel Deaconess Medical Center and Harvard Medical School, Boston, MA, 02215 USA. He is now with Department of Radiology, Icahn School of Medicine at Mount Sinai, New York, NY, 10029-6574 USA

David C. Alsop
Department of Radiology, Beth Israel Deaconess Medical Center and Harvard Medical School, Boston, MA, 02215 USA

Abstract

Functional imaging provides hemodynamic and metabolic information and is increasingly being incorporated into clinical diagnostic and research studies. Typically functional images have reduced signal-to-noise ratio and spatial resolution compared to other non-functional cross sectional images obtained as part of a routine clinical protocol. We hypothesized that enhancing visualization and interpretation of functional images with anatomic information could provide

Correspondence to: Li Zhao.

preferable quality and superior diagnostic value. In this work, we implemented five methods (frequency addition, frequency multiplication, wavelet transform, non-subsampled contourlet transform and intensity-hue-saturation) and a newly proposed ShArpening by Local Similarity with Anatomic images (SALSA) method to enhance the visualization of functional images, while preserving the original functional contrast and quantitative signal intensity characteristics over larger spatial scales. Arterial spin labeling blood flow MR images of the brain were visualization enhanced using anatomic images with multiple contrasts. The algorithms were validated on a numerical phantom and their performance on images of brain tumor patients were assessed by quantitative metrics and neuroradiologist subjective ratings. The frequency multiplication method had the lowest residual error for preserving the original functional image contrast at larger spatial scales (55%–98% of the other methods with simulated data and 64%–86% with experimental data). It was also significantly more highly graded by the radiologists ($p<0.005$ for clear brain anatomy around the tumor). Compared to other methods, the SALSA provided 11%–133% higher similarity with ground truth images in the simulation and showed just slightly lower neuroradiologist grading score. Most of these monochrome methods do not require any prior knowledge about the functional and anatomic image characteristics, except the acquired resolution. Hence, automatic implementation on clinical images should be readily feasible.

Index Terms

magnetic resonance imaging (MRI); arterial spin labeling (ASL); multiple contrasts; visualization enhancement; image similarity

I. Introduction

Magnetic Resonance Imaging (MRI) of the brain with proton density, T1 weighted (T1w), T2 weighted (T2w) and fluid-attenuated inversion recovery (FLAIR) contrast provides outstanding soft tissue contrast and excellent spatial resolution. These methods are widely used for clinical imaging and for research evaluation of lesions, atrophy, and other structural pathologies. More recently, images sensitive to tissue function or molecular activity have been incorporated into clinical research and even routine clinical studies. Techniques such as blood oxygenation contrast [1] for both stimulated and resting state brain activity, dynamic susceptibility contrast for hemodynamic imaging [2], dynamic contrast enhancement for vessel permeability characterization [3] and arterial spin labeling (ASL) [4] for blood flow imaging are all in increasing use for research and clinical protocols. The combination of positron emission tomography with MRI technology [5] also promises to add more functional and metabolic contrasts to the MRI exam. All of these methods share similar features: reduced spatial resolution and signal-to-noise ratio (SNR) relative to structural imaging, difficulty interpreting images with limited anatomic information, and the ease with which spatially registered structural imaging can be acquired in the same study.

In principle, the availability of both functional and anatomic information in a coregistered space provides a wealth of options for combined analysis. In practice, however, medical image based diagnosis is performed by human readers who have limited capability to visually assess multimodal information. Currently, most combined medical image display of

functional and anatomic images involves display of the functional image in color on the anatomic image [6]. There are several limitations of this method. First, color vision may provide more discrimination levels, but luminance vision usually shows superior high frequency structure [7] and shape discrimination [8]. A monochrome image, therefore, may be helpful for the accurate recognition of lesion borders and other key image features. Second, color and brightness information interfere with each other and can be confusing to the observer [9], when anatomic information is provided by luminance and functional information is provided by hue. For example, brightness contrast has been shown to suppress color induction [10]. Third, most commonly with color overlays, threshholding of the functional image and overlaying the superthreshhold voxels on the anatomical image is performed. In such an overlay image, functional imaging information in subthreshold regions is lost and anatomic detail in superthreshold regions is compromised. Disease and potentially patient specific information is also needed to determine an optimal or acceptable threshold. Finally, in most cases, the color-overlay method cannot preserve any quantitative information from the functional images.

Anatomic image information can be used in different ways to improve the information in functional images. Segmentation of anatomic images, along with a priori information about the expected functional signal from different tissue types can be used to correct for volume loss of particular tissue types [11], [12] or to isolate the information of the functional image that is not explained by the spatial distribution of tissue types [13]. Alternatively, anatomic information can be used to guide the reconstruction of images using Bayesian [14], [15] or potentially multi-contrast compressed sensing methods [16]–[18]. Though such methods are promising, they require specialized acquisitions or reconstructions and may make assumptions about the functional image signal, which are not general enough for a broad clinical population. A simpler and more general approach to incorporating anatomic information into functional images would involve combination of images after reconstruction using little or no a priori assumptions about the images.

One important goal for the use of both functional and anatomic image information is to present them in an optimal fashion for the expert interpretation by experienced readers. Such a presentation would enable the maximal use of the inherent visual skills of the experienced eye without confusing the source, either functional or anatomical, of the image features of interest. One promising approach previously proposed [19] for combining functional and anatomic images for medical image display is based on spatial frequency. Because of its lower spatial resolution, the functional image has no intensity in high spatial frequency components. This lack of information can be filled by augmenting the functional image with high spatial frequency information from the anatomical image. As first proposed, simple addition of high spatial frequency information was employed yet the performance of this approach was comparable to the best color based multimodal presentation. Years of development in the field of image fusion has provided algorithms potentially much more powerful than the simple addition used in this pioneering study. Appropriately modified versions of wavelet [20] or contourlet multiscale [21] fusion algorithms, for example, might provide superior results.

The goal of this study is to develop and compare methods for enhancing the visualization and interpretation of low resolution functional images by combining them with high spatial frequency information from anatomical images. Since the target application is image interpretation by skilled medical image readers, subjective scoring by neuroradiologists was emphasized as a quality measure, though quantitative metrics were also assessed. Methods were rated on the degree to which the image combinations improved visualization of overall anatomic location, increased the sharpness of boundaries between lesion and normal tissue, preserved the functional image appearance at larger spatial scales, and produced an overall image quality preferred by the expert.

II. Materials and Methods

A. Image Visualization Enhancement Algorithms

Several approaches to combining functional images, x, with high spatial frequency information from anatomical images, y, were evaluated. Since some of the methods required scaling the anatomical image to the functional image, we define a scaled anatomical image, Y, as

$$Y = y\frac{std(x)}{std(y)} \quad (1)$$

where *std* is the standard deviation of the signal. Other normalization methods, such as histogram matching, are also possible, but in this work we used a linear scaling factor, which is a simple and stable method to match the contrast range of anatomic images to that of functional images, without unpredicted impacts on the performance of visualization enhancement algorithms. This scaling factor is not necessary for frequency multiplication and SALSA methods as shown below. In practice, the functional and anatomic images were scaled by its standard deviation separately, to keep the input data of each algorithm consistent.

1) Frequency Addition Method (FA)—The FA method [19] assumes that the low frequency component of the functional images contains its contrast information. The missing high-resolution information can be provided by the high frequency components of the anatomic image and added after an appropriate scaling.

In this work, a 3D low pass filter (LP) was applied to the frequency space of the functional images and a complementary high pass filter (HP) was applied to the frequency space of the anatomic images. The low pass filter was chosen as Gaussian shape with full width at half maximum (FWHM) that can preserve the acquired resolution of the functional images. Filtered images were added together in frequency space and inverse Fourier transformed to obtain visualization enhanced images (F).

$$F=LP(x)+HP(Y) \quad (2)$$

2) Frequency Multiplication Method (FM)—Similar to the FA method, the high frequency component of the anatomic image can also be extracted by division and combined with functional images by multiplication [22], [23]. The high frequency information is extracted by dividing the anatomic image by a low pass filtered version of the same image. We chose a Gaussian shaped low pass filter as used in the FA method. Pixels in the low pass filtered anatomic image were thresholded to be at least 1% of its mean value to reduce the potential amplification of noise. This value was chosen empirically in this work. A better way to decide the threshold value should consider the SNR and contrast of images.

$$F=x\frac{y}{LP(y)} \quad (3)$$

3) ShArpening by Local Similarity with Anatomic images (SALSA)—SALSA is an algorithm developed by the authors drawing from concepts of image similarity and mutual information [24]. Acquired functional images can be conceptually decomposed into two orthogonal parts: one represents the component similar (*S*) with the anatomic image (*y*) and the other is the component dissimilar (*D*). A first order estimate of *S* and *D* can be obtained by vector multiplication.

$$S_0=\frac{\langle x,y\rangle}{\langle y,y\rangle}y \quad (4)$$

$$D_0=X-S_0 \quad (5)$$

<, > is used to represent the inner product operator.

Subsequently, the local similarity is removed from *D* iteratively with index *n*. A local region of anatomic image is selected by a kernel, which is a Gaussian filter and normalized by $\Sigma K = 1$. The local similarity between the crude dissimilar image, *D*, and the selected region of anatomic image, *Ky*, is calculated following Eq. [4]. Then, the local similarity is further removed from the dissimilar image *D*.

$$D_{n+1}=D_n-\varepsilon\left(\frac{\langle Ky,D_n\rangle}{\langle Ky,y\rangle}Ky\right) \quad (6)$$

ε is a relaxation factor less than one, which controls the convergence of the algorithm. In this work, a value of 0.2 was found empirically to perform well and was used for all analyses, but the results were not highly sensitive to this value.

A fast kernel calculation can be performed simultaneously across all kernel positions by using the Fourier transform convolution theorem.

$$D_{n+1}=D_n-\varepsilon\left(K\otimes\frac{K\otimes yD_n}{K\otimes yy}\right)y \quad (7)$$

where, $\otimes$ is convolution operator and is performed by multiplication in frequency space.

D was updated iteratively, until the maximum iteration number was met (N=200) or the improvement upon the current iteration was small.

$$\frac{\langle D_{n+1}-D_n, D_{n+1}-D_n\rangle}{\langle D_n, D_n\rangle}<0.002 \quad (8)$$

By removing the dissimilarity D_n from the original functional image, the visualization enhanced image F preserves most of the similarities between the functional and anatomic images.

$$F=x-D_n \quad (9)$$

4) Wavelet Transform Method (WT)—Wavelet space fusion assumed the image can be separated into approximate and detail components of the wavelet basis by multi-scale transformation. The approximation coefficients represent the low-resolution contrast of the images and the detail coefficients represent the fine structure information. To enhance the visualization of the functional image, we employed the approximation coefficients of the functional image and detail coefficients from both the functional and anatomic images.

The functional and anatomic images were first forward transformed to the wavelet domain separately and decomposed at 3 levels. We used the wavelet basis of 'bior2.2', following prior work [20]. To preserve the contrast of the functional images, the approximation coefficients of the visualization enhanced images were taken from the functional images. For the detail coefficients, the larger of the functional and anatomic coefficients were assumed to represent more noticeable changes at that transformation level, which reflects the salient feature in the images, such as edges between tissues. Therefore, to include the most spatial information, the detail coefficients of the visualization enhanced image were chosen to be the coefficients with the greater magnitude (choose-max) between the functional and anatomic images. Then, the inverse wavelet transform was used to obtain the visualization enhanced images.

$$C_x = WT(x) \quad (10)$$

$$C_Y = WT(Y) \quad (11)$$

$$C_F = \{C_{x,1}, Cmax(C_{x,2}, C_{Y,2}), \cdots, Cmax(C_{x,N}, C_{Y,N})\} \quad (12)$$

$$Cmax(a,b) = \begin{cases} a & if|a| > |b| \\ b & otherwise \end{cases} \quad (13)$$

$$F = WT^{-1}(C_F) \quad (14)$$

5) Nonsubsampled Contourlet Transform Method (NSCT)—Several authors have evaluated the favorable features of the contourlet transform for fusion applications. The non-subsampled contourlet transform [25] uses an overcomplete transform instead of an orthogonal transform and a non-subsampled filter bank instead of a down-sampling operator. Consequently, the NSCT provides a multiscale, multidirection and shift-invariant image fusion method.

Similar to wavelet fusion, images were first forward transformed to the contourlet domain. Here, we used pyramid filters 'pyrexc' and orientation filter 'vt' with [4, 8, 8, 16] levels of decomposition, according to the work of Li et al. [21]. The approximation coefficients of the visualization enhanced image were again from the functional image and the detail coefficients were chosen to be the ones of greater magnitude between the functional and anatomic images. Then, inverse transformation was used to obtain the visualization enhanced images.

$$C_x = NSCT(x) \quad (15)$$

$$C_Y = NSCT(Y) \quad (16)$$

$$C_F = \{C_{x,1}, Cmax(C_{x,2}, C_{Y,2}), \cdots, Cmax(C_{x,N}, C_{Y,N})\} \quad (17)$$

$$F=NSCT^{-1}(C_F) \quad (18)$$

6) Intensity-Hue-Saturation Method (IHS)—We also evaluated a color overlay method, which is often used to combine anatomic and functional information in neuroradiology. One early work from Levin [6] generated combined images by using the intensity of the anatomic image and the hue of the functional image. This idea was further developed into Intensity-Hue-Saturation based methods [26], which fuse colored images in IHS space instead of RGB space and result in high spectral quality.

In our implementation of the IHS method, the functional images were transferred to pseudo RGB space based on the 'hot' color map of MATLAB (Mathworks, Natick MA). The brightness and contrast of anatomic images were adjusted to match the functional images with a linear transformation [27]. With gray-scale anatomic images, the visualization of pseudo-colored functional images were enhanced in IHS space as described in Eq. [5] of Tu et al. [28].

B. Numerical Phantom and Evaluation

Though the visualization enhancement algorithms are not expected to produce true high resolution functional images, an optimal algorithm should be expected to approximate a high resolution functional image when the information in the anatomic and functional image are similar. It is difficult to assess the visualization enhancement of an algorithm quantitatively without true high-resolution functional images, which are usually unachievable in a practical scan. To evaluate the performance of the proposed methods in a controlled condition, we generated a numerical 3D ASL image phantom by tissue segmentation of an in-vivo high-resolution anatomical image of the brain. High resolution anatomic images were obtained from an open database [29] (case 4). T1w images, T2w images and FLAIR images were used as anatomic references in this study.

The Statistical Parametric Mapping brain imaging analysis software (SPM12, Wellcome Institute of Cognitive Neurology) was used to segment T1w images into gray matter (GM), white matter (WM), cerebrospinal fluid (CSF), bone and soft tissue, based on an extended set of tissue probability maps [30]. To obtain a contrast similar to an ASL cerebral blood flow image, GM of the segmented images was assigned a blood flow value 70ml/100g/min, and WM was assigned 20ml/100g/min. All other regions were removed from the numerical phantom. We smoothed the phantom by a Gaussian convolution kernel (the kernel size was 3mm×3mm×3mm and standard deviation was 0.6mm) to avoid unrealistically sharp transitions. This phantom simulated a high-resolution cerebral blood flow image and it was referred to as the ground truth ASL image in the evaluation.

To replicate the image quality in a practical ASL scan, ideal ASL images were Fourier transformed and filtered by a 3D Gaussian low-pass-filter, which resulted in a resolution of 8mm×8mm×8mm. Complex white Gaussian noise was added to Fourier space resulting in a SNR of 20 within GM. These images were treated as a simulation of the lower quality ASL blood flow image typically acquired.

The anatomic information can be provided by T1w images, but other MR contrasts can also provide additional information. We registered T2w and FLAIR images to T1w images and used them as alternative sources of anatomic information.

The lower quality ASL blood flow image was processed using the 5 monochrome and IHS visualization enhancement methods above with different anatomic images. The low pass filter in FA, FM and SALSA was chosen according to the resolution of ASL. The resulting visualization enhanced images were evaluated by comparing to the ground truth ASL. Root mean squared error (RMSE) relative to the ideal image was calculated in arbitrary units. Another proposed method for assessing image quality degradation, the structural similarity (SSIM) [31], was calculated.

Our image visualization enhancement algorithms were targeted to improve the visual interpretation, and also to preserve the original contrast of the acquired low-resolution ASL signal. To verify whether the different visualization enhancement methods achieved this property, we filtered the visualization enhanced image by the same low pass filter to return a low-resolution image that should approximate the acquired low resolution ASL image. The RMSE and SSIM were calculated between the simulated low-resolution ASL images and visualization enhanced ASL blood flow images with low pass filtering. To distinguish this from the earlier described RMSE and SSIM measures, we refer to these metrics as RMSElp and SSIMlp.

C. Clinical Imaging Acquisition and Evaluation

The visualization enhancement algorithms were evaluated in two groups of patients with high grade glioma. The first group of four patients with high grade malignant glioma were selected from a clinical database following an approved, consent waived retrospective human subjects research protocol. This group was used for initial evaluation and quantitative characterization of the algorithms. Since different protocols were used for these subjects, sequence parameters were not identical across this group. A second group of seven subjects were part of a study to assess response and cerebral blood flow of recurrent glioblastoma after bevacizumab therapy. These subjects were prospectively imaged according to a protocol approved by the Institutional Review Board (IRB) and informed consent was obtained from all participants. Both anatomic and ASL images were obtained at baseline and two weeks after initiation of bevacizumab treatment at a dose of 10mg/kg. Data from the second group were also used for qualitative evaluation by neuroradiologists.

All scans were performed on 3 Tesla General Electric HDxt MRI scanners. ASL images were acquired with 3D stack of spiral fast spin echo acquisition, pseudo-continuous arterial spin labeling (PCASL) [32], and background suppression. A 1.5s post-labeling delay and 1.5s labeling were employed. Spatial resolution varied between 3.5 and 4mm. Anatomical images were acquired with commercial T1w sequences but with variable scan parameters across subjects in the first group. For the subjects of the second group, much more uniform entry criteria and imaging protocol were used: axial T2 weighted images was acquired with fast spin echo sequence with slice thickness 5mm, 1.5mm gap, in-plane resolution 0.75mm×0.75mm, TR 5.1s, TE 111ms, echo train length 24. T1 weighted images with Gd contrast agent were acquired with an MPRAGE sequence with isotropic resolution

1mm×1mm×1mm, inversion time 920ms, TE 2.0ms, TR 8.4s. T1w FLAIR was acquired with and without contrast agent. Detailed parameters are slice thickness 5mm, 1.5mm gap, in-plane resolution 0.75mm×0.75mm, TE 8.5ms, TR 2.4s. T2w FLAIR was acquired with slice thickness 5mm, 1.5mm gap, in-plane resolution 0.75mm×0.75mm, inversion time 2.2s, TE 131ms, and TR 10s.

Image enhancement requires excellent registration between the functional and anatomic images. An automatic coregistration algorithm employing maximum mutual information implemented in the SPM12 software package was used. Anatomic images with other contrasts, such as FLAIR, T2w images, were coregistered to T1w images, the resolution of which was used in the following tests To improve the registration of functional images, the gray matter of T1w images were segmented according to a probability map. This region has similar contrast as ASL. By registering ASL images to the gray matter, ASL images were also coregistered with T1w images.

In the first group, the visualization enhancement algorithms were performed with anatomic information of T1w images with Gd contrast. The normalized RMSElp (nRMSElp) and the SSIMlp were calculated across subjects to access the preservation of the original quantification information of ASL images.

In the second group, ASL images were processed by the proposed algorithms and using each of the T2w, T2w FLAIR, T1w FLAIR images with and without Gd contrast and 3D MPRAGE with Gd contrast images as the anatomic image. An expert assessment of the image quality was performed by two experienced clinical neuroradiologists. Original and visualization enhanced images were exported to DICOM format anonymously. Two neuroradiologists were asked to adjust the view windows based on experience and grade the acquired and visualization enhanced images with a Likert scale (1 for strongly disagree; 2 for disagree; 3 for neither agree nor disagree; 4 for agree and 5 for strongly agree). Three criteria were evaluated: (1) clear brain anatomy around tumor, (2) clear borders between tumor and normal tissue, and (3) good preservation of ASL blood flow contrast. Additionally, clinician preference for the visualization enhanced ASL image vs the original ASL image was evaluated (1 for preference of the visualization enhanced image and 0 for preference of the original ASL).

The radiologist scores were compared for different algorithms using a two-sided Wilcoxon signed rank test. Pairwised comparisons were performed between FM and each of other method individually and for each criterion separately. The performance of each method was assessed by the average score and standard deviation across subjects, radiologists and different anatomic reference images.

III. Results

A. Evaluation in Numerical Phantom

Figure 1 shows the improved ASL images on the numerical phantom with different methods and using anatomic information from T1w, T2w and FLAIR images. The visualization enhanced images provided more detailed spatial information and more importantly,

maintained the overall contrast of ASL. For example, in T1w images, white matter has higher signal intensity than gray matter, which is opposite to the contrast in ASL images. But, when using the T1w images as anatomic reference, the contrast of the visualization enhanced images was similar to the acquired ASL images at greater than 8mm spatial scales, as shown in Figure 2.

The FA, wavelet and NSCT methods display signal from the scalp in the visualization enhanced image despite its absence in the ideal image. This could be an advantage that provides additional information regarding anatomical position, but also results in less realistic contrast compared with the ideal ASL images.

Figure 2 demonstrates how low pass filtered improved images strongly resemble the initial, low-resolution image. This indicates that the improved images preserved the quantitative ASL information at larger spatial scales and could feasibly be used for quantitative analysis. By visual comparison, low pass filtered FM resulted in the smallest difference from the simulated ASL and it, therefore, most faithfully reproduced the original low-resolution ASL images.

Table I details the quantitative metrics of image quality for the simulation. Of the methods evaluated, the FM and SALSA methods performed best. The SALSA method increased the structural similarity to the ground truth ASL by 11%–133% across methods and anatomic images, while the measures of the difference from ground truth ASL, RMSE, and preservation of low spatial frequency contrast, RMSElp (55%–98% of other methods) and SSIMlp, generally indicated that FM provided the best results across all anatomic reference images used.

Using different anatomic images as reference had a modest effect on enhancement quality. Compared to the ground truth, RMSE and SSIM suggested the best improvement when FLAIR anatomic information was used. Besides enhanced visualization and interpretation, the results suggested further improvement of functional images can be achieved, if accurate high spatial frequency information can be obtained from anatomic images.

B. Evaluation in Clinical Images

Tumor cases in group 1 visualization enhanced using the T1w with Gd as the anatomical reference image are shown in Figure 3. The visualization enhanced images appear sharper and better delineate the tumor boundaries in most of the cases. In case 4, the contrast enhancement and ASL hyperperfusion are very dissimilar and less enhancement occurs. Still, the image with visualization enhancement has better overall anatomic delineation.

Similar to the simulation results, smoothing of the visualization enhanced images produced results very similar to the original ASL image. Among the methods, smoothed FM reproduced the acquired ASL images with the least error (64%–86%) and highest similarity (169%–244%) compared to other methods, as shown in Table II.

Neuroradiologist qualitative scoring of the 7 cases of the second group, Figure 4, confirmed the results of the quantitative simulation analysis. The neuroradiologists scored the FM method as having the best rendering of anatomy (4.7 ± 0.7, $p<0.005$ among the methods),

and the clearest border between tumor and normal tissue (4.1 ± 1.3, $p<0.001$ for all methods except SALSA). The SALSA method provided slightly lower average quality scores, followed by the NSCT, WT and FA methods. All the visualization enhanced images preserved the original blood flow contrast at larger spatial scales and were rated as preferable to the original cerebral blood flow map, except for IHS.

IV. Discussion

This study reported detailed evaluation of several methods to enhance the visualization and interpretation of low resolution functional images through the incorporation of information from higher resolution anatomical images. Simulations and evaluations in clinical images suggest that several techniques were successful at this purpose and preserving the quantitative information. The FM method performed the best at reproducing the true image in simulations, preserving the low resolution contrast of the original ASL images and produced highly rated image quality in clinical evaluations. The SALSA method performed comparably to FM and with a higher SSIM score in the simulations, but it did demonstrate a tendency to contaminate low frequency signal in the clinical evaluation, as evidenced by higher RMSElp. Further refinements to address this weakness may be worth pursuing. Most of the monochrome methods required only specification of the kernel FWHM, which is closely linked to the acquired image resolution. Hence, automatic implementation on clinical imagers should be readily feasible. The proposed method was demonstrated on ASL images, but it could be generalized to enhance the visualization of other contrasts in MRI and multiple image modalities (e.g. PET and MRI).

A previously suggested metric, the fusion assessment score, has been used to demonstrate that the NSCT algorithm provides the best fusion results [21]. In our study, however, the FM and SALSA methods consistently outperformed the NSCT algorithm in our simulation and neuroradiologist ratings. This discrepancy may reflect the different goals of conventional fusion, which aims to mix information from both images, and our visualization enhancement, which sought to preserve functional image contrast at larger spatial scales.

Anatomic images with different contrast can be used for visualization enhancement as shown in simulation and experiments. Not unexpectedly, those anatomic images with contrast more similar to the functional images will provide the most dramatic enhancement, because the high spatial frequency information provided by the anatomic images was similar to what was missing in the ASL images. In the simulation, FLAIR, which has contrast more similar to ASL images in normal subjects, provided the best enhancement; T2 weighted images emphasize CSF, which has no signal on blood flow images, resulting in less satisfying enhancement. The quality of the anatomic images will also play an important role in enhancement. Higher SNR and clearer contrast in the anatomic image will likely achieve better functional image enhancement.

Though the inclusion of anatomical information enhanced the appearance of the ASL images, the accuracy of blood flow representation is limited. High resolution features of the anatomical images will appear in the visualization enhanced functional images to some degree. To the extent that the blood flow signal is expected to actually follow the anatomical

features, for example at gray matter white matter boundaries in FLAIR images, or at tumor edges in contrast enhanced T1w images, these high resolution features may represent blood flow. In other cases, such as bright vessels in contrast enhanced T1w images, or even skull and scalp features in some of the visualization enhancement algorithm results, these high resolution features are unrelated to function. Still, with proper understanding of the anatomic image contributions to the visualization enhanced image, these features can provide anatomical context. Furthermore, when used in a clinical context, such as determining tumor recurrence, seizure activity, or sensorimotor disturbance in patients, these visually enhanced images may need to be viewed in combination with raw functional or anatomical images to fully understand the clinical relevance of particular image features.

Our display algorithm is just one of many ways to use anatomic information to interpret functional images such as ASL. For example, adjusting functional images for tissue loss is frequently considered in the interpretation of functional scans in aging [12]. This adjustment is performed based on a tissue probability map, obtained from high resolution image [11]. Such adjustments are valuable in the analysis of aging and dementia, for example, if images of sufficient quality to segment tissues are available. In clinical practice, however, many pathologies cause flow changes that deviate from the assumptions of the partial volume model. Images from clinical patients with lesions and prior surgery may also be challenging to meaningfully segment, at least without expert supervision. The absence of partial volume correction in our algorithm reflects the goal of simple and broad applicability in clinical practice, hopefully even outside the brain. We should also note that the model used for partial volume correction, when appropriate, can also be used to improve the resolution and SNR of functional images, as in reference [11] figure 5, 4th row.

Spatial coregistration of the functional and anatomic images is essential to the visualization enhancement algorithms. In the absence of subject motion, scans performed during one scanning session should already be spatially registered, though reslicing of the images may be required to match orientation and resolution. We employed an automatic coregistration algorithm that simultaneously matched orientation and corrected for motion between image acquisitions. Should coregistration be necessary for clinical applications, its speed and robustness will be important for the successful enhancement of functional images. In addition, some MRI acquisition methods, such as echo planar imaging, can experience geometric distortion that would require correction prior to performance of the visualization enhancement algorithms [33].

The chosen scale factor for relating functional and anatomical images may impact the performance and robustness of some of the algorithms. Since the FM and SALSA methods employ only multiplication and division, relative scaling of the two images has no effect. This scale independence is an advantage for automatic implementation. For the other methods, a scale factor is required. The standard deviation method used in this study may be not robust to different contrast anatomic images, and other scalings based on nonlinear transform or histogram methods may improve the contrast of anatomic images and provide further visualization enhancement of functional images. Regardless of the scaling, anatomic images with different contrast will contain different anatomic information. The selection of the best type of anatomic image may well depend on the objective of the imaging evaluation.

With additional prior knowledge, the anatomic image could be transformed to a similar contrast as the functional image, for example by nonlinear intensity transformation and segmentation. However, such prior knowledge may not be reliable in a broad clinical or research setting. For this reason, inclusion of prior information was not included in our algorithms.

Multi-scale and multi-channel fusion are active and sophisticated areas of investigation and it is likely that including new developments may increase the quality and relative performance of different algorithms. For example, in this work, we employed a widely used 'choose-max' as the combination method for wavelet and NSCT fusion. Better results have been reported by using area-based activation level selective methods [20], [34], but exhaustive exploration of all possible methods is beyond the scope of this work.

Our newly proposed SALSA method was slightly outperformed by the simpler FM method, but it has several characteristics that make it worthy of further development. It scored better on similarity measures than FM (Table I), perhaps because of its emphasis on a local similarity. Because it is iterative, it may also be possible to perform in cycles across multiple anatomical reference images with different contrast so as to better match functional and anatomic information.

The FWHM of selective kernel K in SALSA is worthy of further investigation besides the effect of a low pass filter. With a larger FWHM, it appeared to perform an edge preserving denoising using the information of the anatomic image. On the other hand, an over-small kernel could result in ring like artifacts. The FWHM of kernel K of SALSA and the low pass filter of FA and FM, were empirically selected according to the resolution of the functional and anatomic images in this work. For example, some anatomic images in the second group, such as FLAIR, were low resolution in the slice direction, which would only improve the ASL images for in-plane dimensions. The detailed performance of the FWHM of kernel, and also the shape of kernel, will need further assessment.

V. Conclusion

In this work, we evaluated methods for enhancing visualization and interpretation of functional images by including spatial information from anatomic images. The resulting images improved visual interpretation while maintaining the original quantification information of the functional images. The methods proposed in this work can be adapted for other modalities, require limited information regarding the original images and can be readily implemented for automatic operation.

Acknowledgments

This work was supported in part by the National Institute of Mental Health through R01MH080729.

References

1. Ogawa S, Lee TM, Nayak AS, Glynn P. Oxygenation-sensitive contrast in magnetic resonance image of rodent brain at high magnetic fields. Magnetic Resonance in Medicine. 1990; 14(1):68–78. [PubMed: 2161986]

2. Rempp KA, Brix G, Wenz F, Becker CR, Gückel F, Lorenz WJ. Quantification of regional cerebral blood flow and volume with dynamic susceptibility contrast-enhanced MR imaging. Radiology. Dec; 1994 193(3):637–41. [PubMed: 7972800]
3. Roberts HC, Roberts TP, Brasch RC, Dillon WP. Quantitative measurement of microvascular permeability in human brain tumors achieved using dynamic contrast-enhanced MR imaging: correlation with histologic grade. AJNR American journal of neuroradiology. May; 2000 21(5): 891–899. [PubMed: 10815665]
4. Detre JA, Leigh JS, Williams DS, Koretsky AP, Leight JS. Perfusion imaging. Magnetic Resonance in Medicine. Jan; 1992 23(1):37–45. [PubMed: 1734182]
5. Judenhofer MS, Wehrl HF, Newport DF, Catana C, Siegel SB, Becker M, Thielscher A, Kneilling M, Lichy MP, Eichner M, Klingel K, Reischl G, Widmaier S, Röcken M, Nutt RE, Machulla HJ, Uludag K, Cherry SR, Claussen CD, Pichler BJ. Simultaneous PET-MRI: a new approach for functional and morphological imaging. Nature medicine. Apr; 2008 14(4):459–65.
6. Levin DN, Pelizzari Ca, Chen GT, Chen CT, Cooper MD. Retrospective geometric correlation of MR, CT, and PET images. Radiology. 1988; 169:817–823. [PubMed: 3263666]
7. Hemminger BM. Isoluminance: a color technique for visualizing multivariable medical image data. Proceedings of SPIE. 1993; 1897:325–335.
8. Mullen KT, Beaudot WHA. Comparison of color and luminance vision on a global shape discrimination task. Vision Research. 2002; 42(5):565–575. [PubMed: 11853774]
9. Moutoussis K. The physiology and psychophysics of the color-form relationship: A review. Frontiers in Psychology. Nov.2015 6:1–17. [PubMed: 25688217]
10. Gordon J, Shapley R. Brightness contrast inhibits color induction: evidence for a new kind of color theory. Spatial vision. Jan; 2006 19(2–4):133–46. [PubMed: 16862836]
11. Asllani I, Borogovac A, Brown TR. Regression algorithm correcting for partial volume effects in arterial spin labeling MRI. Magnetic Resonance in Medicine. 2008; 60(6):1362–1371. [PubMed: 18828149]
12. Asllani I, Habeck C, Borogovac A, Brown TR, Brickman AM, Stern Y. Separating function from structure in perfusion imaging of the aging brain. Human brain mapping. Sep; 2009 30(9):2927–35. [PubMed: 19172645]
13. Kandel BM, Wang DJJ, Detre JA, Gee JC, Avants BB. Decomposing cerebral blood flow MRI into functional and structural components: a non-local approach based on prediction. NeuroImage. Jan. 2015 105:156–70. [PubMed: 25449745]
14. Kornak J, Young K, Schuff N, Du A, Maudsley Aa, Weiner MW. K-Bayes reconstruction for perfusion MRI. I: concepts and application. Journal of Digital Imaging. Jun; 2010 23(3):277–86. [PubMed: 19205805]
15. Kornak J, Young K. K-Bayes reconstruction for perfusion MRI II: modeling and technical development. Journal of Digital Imaging. Aug; 2010 23(4):374–85. [PubMed: 19274427]
16. Zhao L, Fielden SW, Feng X, Wintermark M, Mugler JP, Meyer CH. Rapid 3D dynamic arterial spin labeling with a sparse model-based image reconstruction. NeuroImage. Jul.2015 121:205–216. [PubMed: 26169322]
17. Bilgic B, Goyal VK, Adalsteinsson E. Multi-contrast reconstruction with Bayesian compressed sensing. Magnetic resonance in medicine. Dec; 2011 66(6):1601–1615. [PubMed: 21671267]
18. Wright KL, Ma D, Jiang Y, Gulani V, Griswold MA, Hernandez-Garcia L. Theoretical Framework for MR Fingerprinting with ASL: Simultaneous Quantification of CBF, Transit Time, and T1 Katherine. Proc Intl Soc Mag Reson Med. 2014; 22:417.
19. Quarantelli M, Alfano B, Larobina M, Tedeschi E, Brunetti A, Covelli EM, Ciarmiello A, Mainolfi C, Salvatore M. Frequency encoding for simultaneous display of multimodality images. Journal of Nuclear Medicine. 1999; 40(3):442–7. [PubMed: 10086709]
20. Pajares G, Manuel de la Cruz J. A wavelet-based image fusion tutorial. Pattern Recognition. Sep; 2004 37(9):1855–1872.
21. Li S, Yang B, Hu J. Performance comparison of different multi-resolution transforms for image fusion. Information Fusion. 2011; 12(2):74–84.
22. Filiberti DP. Synthesis of imagery with high spatial and spectral resolution from multiple image sources. Optical Engineering. 1994; 33(8):2520–2528.

23. Hill J, Diemer C, Stöver O, Udelhoven T. A local correlation approach for the fusion of remote sensing data with different spatial resolutions in forestry applications. International Archives of Photogrammetry and Remote Sensing. 1999; 32:3–4.
24. Zhao L, Dai W, Alsop DC. Arterial Spin Labeling Improvement by Incorporating Local Similarity with Anatomic Images. Proc Intl Soc Mag Reson Med. 2015; 23:2325.
25. da Cunha AL, Zhou J, Do MN. The nonsubsampled contourlet transform: theory, design, and applications. IEEE Transactions on Image Processing. 2006; 15(10):3089–3101. [PubMed: 17022272]
26. Rahmani S, Strait M, Merkurjev D, Moeller M, Wittman T. An adaptive IHS pan-sharpening method. IEEE Geoscience and Remote Sensing Letters. 2010; 7(4):746–750.
27. Gonzalez, RC., Woods, RE. Digital image processing. Prentice Hall; 2002.
28. Tu TM, Su SC, Shyu HC, Huang PS. A new look at IHS-like image fusion methods. Information Fusion. 2001; 2(3):177–186.
29. Landman BA, Huang AJ, Gifford A, Vikram DS, Lim IAL, Farrell JAD, Bogovic JA, Hua J, Chen M, Jarso S, Smith SA, Joel S, Mori S, Pekar JJ, Barker PB, Prince JL, van Zijl PCM. Multi-parametric neuroimaging reproducibility: a 3-T resource study. NeuroImage. Feb; 2011 54(4): 2854–2866. [PubMed: 21094686]
30. Ashburner J, Friston KJ. Unified segmentation. NeuroImage. 2005; 26(3):839–851. [PubMed: 15955494]
31. Wang Z, Bovik AC, Sheikh HR, Simoncelli EP. Image quality assessment: from error visibility to structural similarity. IEEE Transactions on Image Processing. Apr; 2004 13(4):600–612. [PubMed: 15376593]
32. Dai W, Garcia D, de Bazelaire C, Alsop DC. Continuous Flow-Driven Inversion for Arterial Spin Labeling Using Pulsed Radio Frequency and Gradient Fields. Magnetic Resonance in Medicine. Dec; 2008 60(6):1488–1497. [PubMed: 19025913]
33. Jezzard P, Balaban RS. Correction for geometric distortion in echo planar images from B0 field variations. Magnetic Resonance in Medicine. Jul; 1995 34(1):65–73. [PubMed: 7674900]
34. Li, H., Manjunath, B., Mitra, SK. Multisensor Image Fusion Using the Wavelet Transform. 1995. p. 235-245.

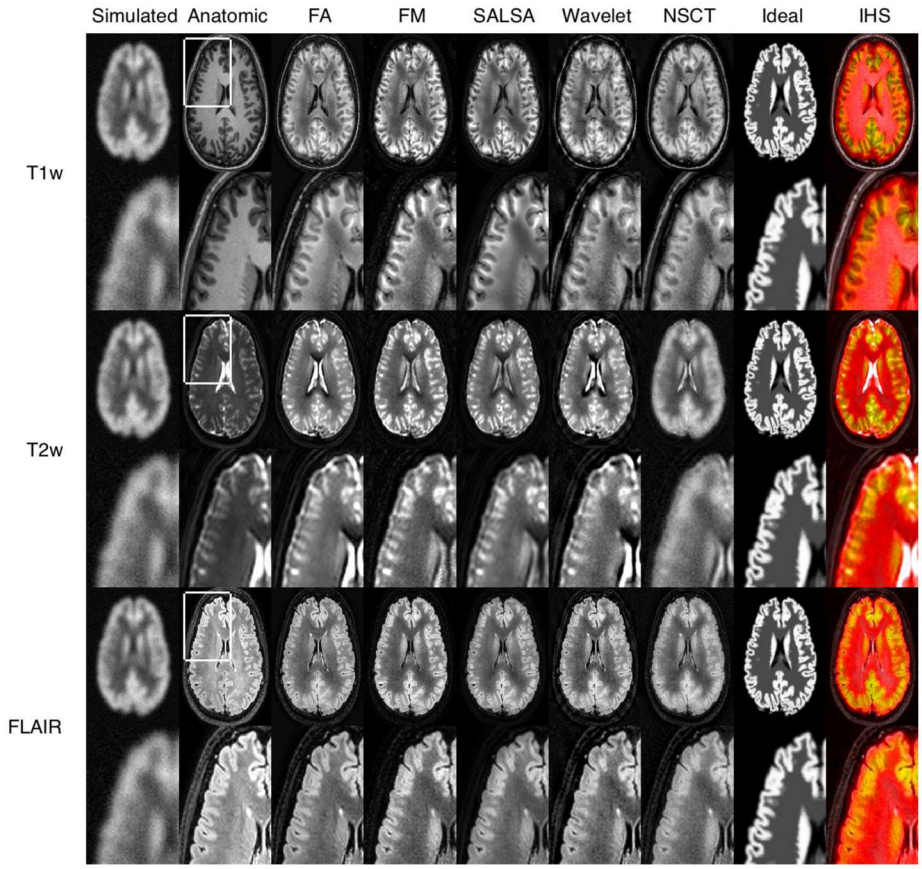

Fig. 1.

Comparison of image visualization enhancement methods performed on the numerical phantom. Results from one selected slice and zoomed-in sections are shown with different anatomic reference images and different enhancement methods.

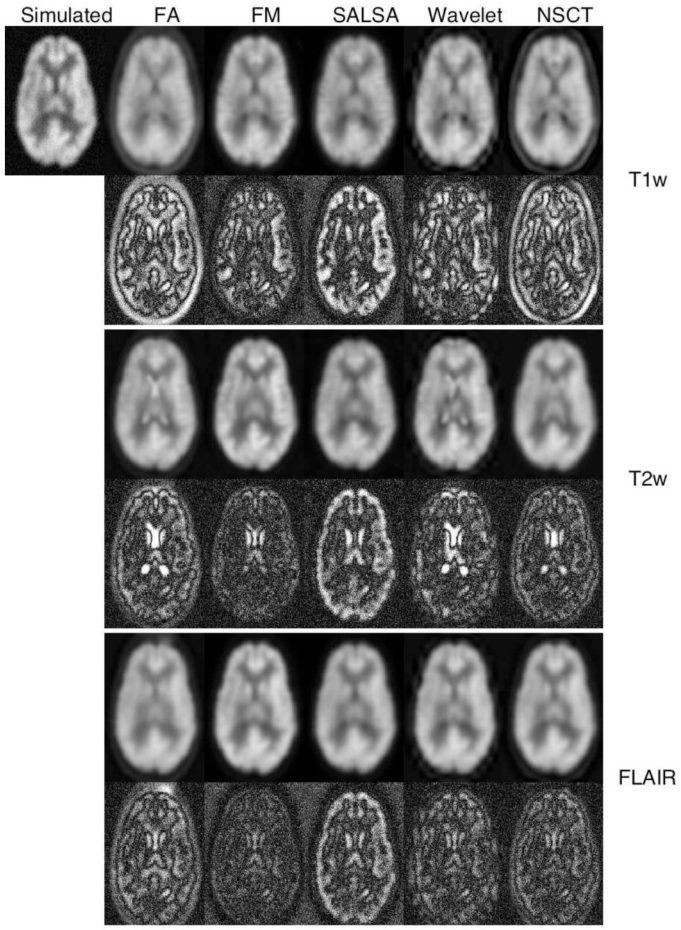

Fig. 2.

The low frequency component of the visualization enhanced images. Top rows are the low-resolution component of the visualization enhanced images and the bottom rows are the absolute difference (×5) from the simulated low resolution ASL image.

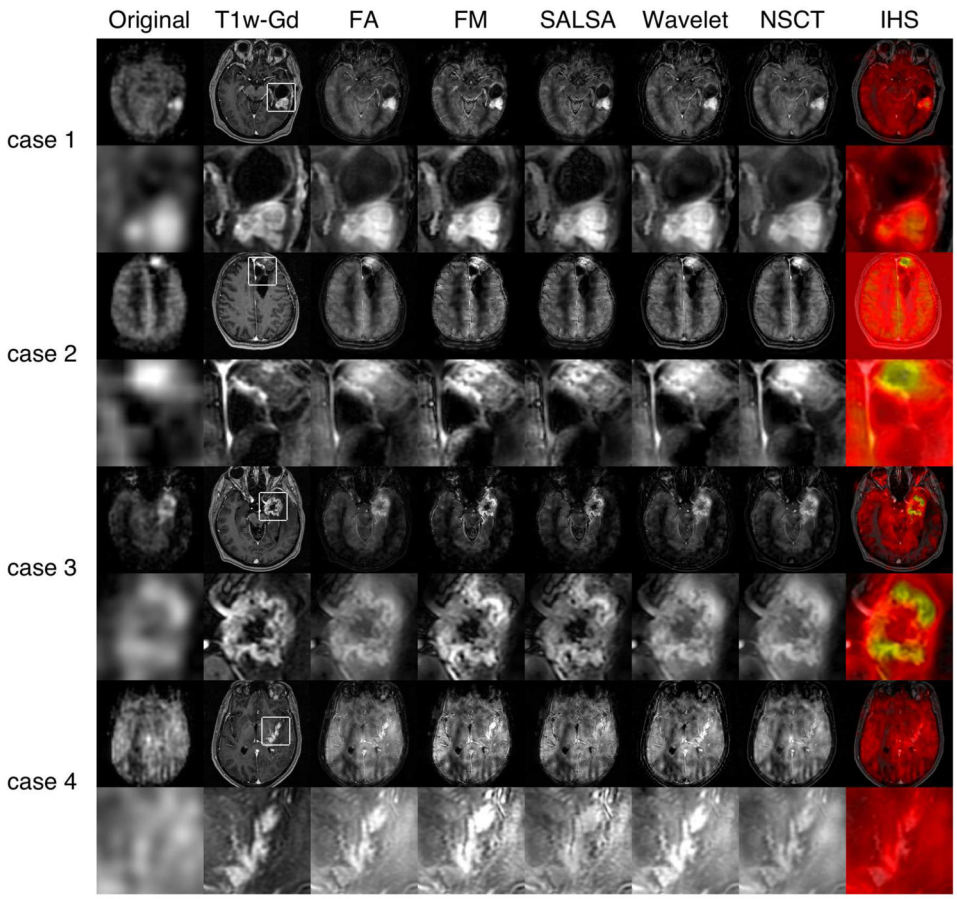

Fig. 3.

Application of the different image visualization enhancement methods to ASL images obtained from patients with high grade glioma (from group 1). Contrast enhanced T1 weighted images were used as the anatomic image in the algorithms.

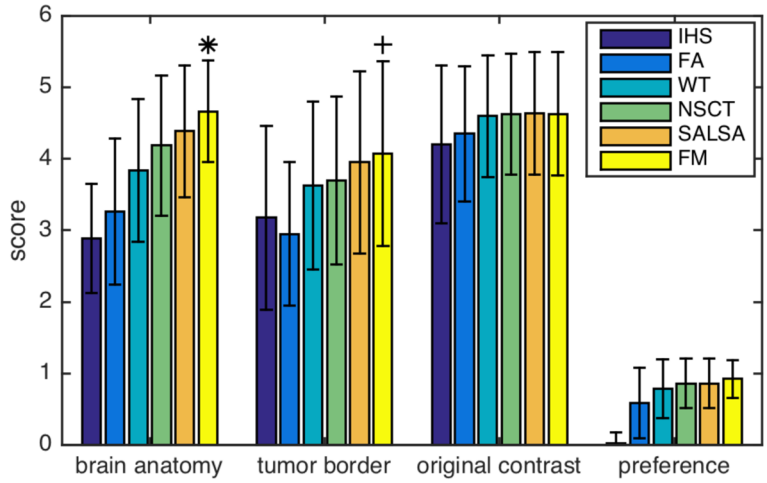

Fig. 4.

Neuroradiologist rating scores. The error bar shows the standard deviation across subjects, anatomic images and radiologists. * FM showed significantly higher scores for brain anatomy compared to other methods (IHS, FA, WT, NSCT $p<0.001$ and SALSA $p<0.005$). + FM showed significantly higher scores for tumor border compared to other methods (IHS, FA, WT and NSCT $p<0.001$), except SALSA ($p=0.07$).

TABLE I

Quantitative measures of visualization enhancement quality and fidelity in the simulation study

		FA	FM	SALSA	WT	NSCT
T1w	RMSE	0.2100	**0.1694**	0.1740	0.1971	0.1829
	SSIM	0.1836	0.3581	**0.4277**	0.2192	0.2990
	RMSElp	0.0910	**0.0505**	0.0666	0.0664	0.0512
	SSIMlp	0.7077	**0.8236**	0.7613	0.7765	0.7639
T2w	RMSE	0.2041	0.1650	0.1623	0.2003	**0.1573**
	SSIM	0.2538	0.3291	**0.3901**	0.2657	0.3035
	RMSElp	0.0715	**0.0423**	0.0601	0.0584	0.0512
	SSIMlp	0.8033	**0.8771**	0.8486	0.8301	0.8534
FLAIR	RMSE	0.1530	**0.1134**	0.1239	0.1452	0.1349
	SSIM	0.3478	0.5070	**0.5612**	0.3632	0.3827
	RMSElp	0.0663	**0.0413**	0.0583	0.0517	0.0485
	SSIMlp	0.8003	0.8232	0.7806	0.8379	**0.8467**

RMSE root of mean squared error between improved and ideal images.

SSIM structural similarity between improved and ideal images.

RMSElp root of mean squared error between original and low resolution component of visualization enhanced images.

SSIMlp structural similarity between original and low resolution component of visualization enhanced images.

TABLE II

Quantitative measures of difference and similarity between the original ASL images and the low resolution component in visualization enhanced ASL images in glioma patients of group 1.

	FA	FM	SALSA	WT	NSCT
nRMSElp	0.28 ± 0.01	**0.18 ± 0.02**	0.22 ± 0.03	0.28 ± 0.01	0.21 ± 0.03
SSIMlp	0.31 ± 0.01	**0.66 ± 0.07**	0.39 ± 0.03	0.27 ± 0.02	0.28 ± 0.02

nRMSElp normalized error between original and low resolution component of visualization enhanced images

SSIMlp structural similarity between original and low resolution component of visualization enhanced images